(141). These tests were carried out in order to establish the level of applied alternating stress intensity required for crack growth rates in excess of 1 $x10^{-7}$ m/cycle. Any ductile striations present in the resulting fatigue-fracture surfaces would be easily resolvable at these growth rates.

From the results of these initial tests, three levels of (nominally) constant K were chosen for specimens W2 (welded) and P4 (parent plate); namely 50, 55 and 60 MPa $\sqrt{m}$. In both of these tests, a programmed load change was used to beachmark the fracture surfaces of the specimens in between each constant Δ K level, and these fracture surfaces are shown in Figure 7.13. It can be seen from this Figure that the crack front curvature was much more pronounced in the weld metal specimen (W2) than in the parent plate specimen (P4). As detailed in Section 7.1.4, welding residual stresses (although not great in magnitude in specimens of this size) are the main factor in causing this uneven growth, and it is to be expected that there will be more crack curvature in the welded samples than in the parent plate material.

Fatigue crack growth rates were calculated using the ASTM recommended secant method (142) for each specimen from the two optical readings, as well as from the potential drop readings. The results obtained for specimen W2 (weld metal) are shown in Figure 7.14 (a) and (b); two graphs were plotted for this specimen, due to the extent of uneven crack growth observed during the test. The positions of the beachmarks (i.e. the crack lengths at which the applied stress intensity was changed) are indicated on these diagrams by vertical lines; these beachmarks clearly illustrate the difference observed in the two optical crack length measurements (Figure 7.14). Furthermore, it can be seen from Figure 7.14 that there is some considerable scatter in the calculated growth rates, for each level of (constant) applied stress intensity. However, the <u>average</u> level of fatigue crack growth rate within each block does increase with increasing stress intensity.

The crack growth rate, as calculated from the potential drop measurements are also shown on each graph for comparison. It can be seen that the potential drop appears to follow the trend of the optical measurements, but with some variability. However, it must be remembered that this technique measures the <u>average</u> value of fatigue crack length, and therefore the scatter between the optical and potential drop growth rates in these two Figures is easily understood.

The corresponding crack growth rates evaluated for specimen P4 (parent plate) are shown in Figure 7.15, and it will be seen that the scatter is much reduced, as compared to Figures 7.14 (a) and (b). It will be recalled from Section 7.2 that the crack lengths recorded on each side of this specimen were very consistent, and this is reflected in the crack growth rates. In addition, the amount of scatter in the growth rates evaluated for each level of constant ΔK is much reduced. The crack growth rate evaluated from the potential drop measurements appears, in the final stage, to overestimate the crack growth rate, but again this is much less that the scatter observed for specimen W2, as indeed would be expected, since there was much less crack bowing in the parent plate specimen (as shown in Figure 7.13).

The crack growth rates evaluated for each specimen were plotted against the applied alternating stress intensity (calculated as recommended in the ASTM standard (142)) in the conventional log-log form, as shown in Figure 7.16. These graphs also show the scatterband obtained in the initial constant load tests for each specimen type. The uneven crack growth observed in specimen W3 is again indicated in these results, with considerably more scatter in Figure 7.16 (a) than for the corresponding results of the parent plate specimen, shown in Figure 7.16 (b). This scatter is most clearly illustrated by the fact that the results obtained for the weld metal specimen apparently fall on the same curve, whereas the results of the parent plate specimen do in fact show the three different levels of nominally constant stress intensity that were applied during the test, and the corresponding three levels of fatigue crack growth. There is some variability between the optical crack growth rates and those measured using the potential drop system; on the whole, however, these Figures both indicate the usefulness of the potential drop technique for crack length monitoring in this type of test.

Specimens W3 (welded) and P5 (parent plate) were tested at nominally constant applied alternating stress intensities of 30, 35, 40, 45, 65 and 70 MPa $\sqrt{m}$. The specimen fracture surfaces are shown in Figure 7.17, and it can be seen that the crack curvature in specimen W3 is greater at the low stress intensities than at the higher levels of ΔK. However, as detailed in Section 7.1.4, one of the associated causes of crack curvature is due to the fact that whereas the centre of the specimen is in plane strain (at low loads), the edges are in a state of plane stress. At higher stresses, it can be expected that the regions of plane stress will extend further into the specimen, thereby reducing the extent of crack bowing. Additionally, of course, the welding residual stresses (the main cause of curvature) are likely to be less dominant at the higher stresses. Comparing Figure 7.17 with Figure 7.13, it is clear that there was no extensive uneven growth in specimen W3. This is due to the fact that welding residual stresses will not be the same from specimen to specimen; in addition there are likely to be microstructural differences along the weld, and thus between specimens cut from the weld.

The results obtained in the evaluation of the crack growth rates in the welded specimen (W3) and the parent plate specimen (P5) are shown in Figure 7.18 and 7.19, respectively. It can be seen that there is some scatter in these results, notwithstanding the compatibility between the crack length measurements obtained in these two specimens. It is therefore worth considering possible sources of experimental error in measuring crack lengths, since these will obviously affect the calculation of crack growth rates. The optical methods used for surface crack length measurement are inherently less reliable than a properly calibrated potential drop system, since any error in accurately locating the crack tip will affect two crack growth rate calculations. As previously indicated, the secant method was used to calculate the growth rates:-

$$\frac{da}{dN} = \frac{(a_{i+1} - a_i)}{(N_{i+1} - N_i)} \qquad (7.3)$$

Thus, if a_{i+1} is underestimated, the crack growth rate for that interval will be underestimated, and the growth rate of the subsequent interval will be overestimated. Clearly, this can have a considerable effect at lower growth rates. Additionally, of course, the fatigue crack extension will not be uniform across the crack front, and this can lead to errors in the calculation of the crack growth rate, even if the crack tip on each side is accurately located. However, it is considered that since the crack growth was monitored on each side, as well as via the potential drop, sufficient data was indeed obtained, for the purposes of this particular investigation.

The crack growth rates obtained in specimens W3 and P5 were plotted against the cyclic stress intensity, as shown in Figure 7.20. It is clear that the reduced level of crack curvature observed in specimen W3 has resulted in more accurate test results, with the six different ΔK levels clearly apparent in Figure 7.20 (a). (This should be compared to the results shown in Figure 7.16 (a), where the uneven crack growth makes it difficult to distinguish the three nominal constant ΔK levels used in this test). However, there is some considerable scatter in the crack growth rates measured in this weld metal specimen at the nominal stress intensities of 30 and 35 MPa$\sqrt{m}$, as shown in Figure 7.20 (a). It is considered that this is due to the low growth rates that are being measured; where any errors in measuring crack lengths will be reflected in a wide scatter band of crack growth rates. Additionally, as noted above, at these low growth rates the crack extension will not be uniform across the crack front, especially for the relatively small number of loading cycles between each measurement. The data shown in Figure 7.20 (b), on the other hand indicates that the fatigue crack growth rate in the parent plate specimen is in excess of 1 x 10^{-7} m/cycle for these same levels of applied stress intensity.

This may therefore indicate that the weld metal has a higher resistance to fatigue crack propagation than the parent plate, which obviously is an ideal condition for a welded structure. However, it could also be due to the fact that the welding residual stresses affect the growth rate at the low stress intensities, but become ineffectual at the higher levels of applied stress.

7.3.2 Correlation of striation spacing with crack growth rate

The fatigue portion of the fracture surfaces shown in Figures 7.13 and 7.17 were cut from each specimen, mounted on stubs and a grid was scribed on the surface, as shown in Figure 7.21. (This was to enable easy identification of the locations which were studied at high magnifications). In order to correlate the observed macroscopic growth rates with the striation spacings, the specimens were scanned up each side, and in the centre, in the direction of crack propagation. As discussed in the preceding section, there was some variability in the crack growth rates as measured from each side, as well as between the optical and the electrical measurements. It was therefore considered that the assessment would be incomplete if only one scan was made along the fracture surface.

Striations could not be resolved at cyclic stress intensities less than 45 MPa$\sqrt{m}$ in either the weld metal, or in the parent plate, corresponding to growth rates less than 1×10^{-7} and 5×10^{-7} m/cycle, respectively. Indeed, even at the higher stress intensities, the striations generally tended to occur in "packets" and were not that well defined, as shown in Figure 7.22. In addition, the striation spacing could vary significantly within a small area, as shown in Figure 7.23, where there appear to be coarse and fine striations within close proximity. For the region shown in Figure 7.23 (a), the macroscopic growth rate was measured at $1,20 \times 10^{-6}$ m/cycle, whereas the coarse and fine striations represent growth rates of $1,24 \times 10^{-6}$ and $4,66 \times 10^{-7}$ m/cycle, respectively. In the region shown in Figure 7.23 (b), the measured macroscopic growth rate was $2,5 \times 10^{-6}$ m/cycle, whereas the coarse and fine striations represent growth rates of $1,15 \times 10^{-6}$ and $3,5 \times 10^{-7}$ m/cycle respectively.

Consistent with the work of Lankford and Davidson (28), fine striations were observed, in some cases, to be sub-units of the coarse striations as shown in Figure 7.24. Preliminary comparisons with the local growth rates, however, (such as those in the preceding paragraph) indicated that the coarse striations were more representative of the macroscopic conditions. At the high stress intensities, the striations were interspersed in areas that had otherwise fractured almost completely due to ductile void coalesence (Figure 7.25), thus indicating the importance of "static modes" in fatigue failure. These microscopic features all contributed to the overall difficulty of this work.

However, there were some relatively large areas of well defined ductile striations, as evidenced in Figure 7.26; the regions shown in this Figure were observed in the welded specimen (W2) and were associated with cyclic stress intensity levels of between 50 and 55 MPa$\sqrt{m}$.

The results obtained in the comparison of fatigue striation spacings and the observed macroscopic growth rates in specimen W2 and W3 are shown in Figures 7.27 (a) and (b) respectively. These results indicate that, for the levels of cyclic stress intensity used in this investigation, the striation spacing <u>never</u> overestimates the observed macroscopic growth rates for the weld metal specimens. Indeed, the striation spacing tends, on the whole to underestimate the fatigue cack propagation rate, and there are only a few instances of the two parameters coinciding. Such instances are particularly evident in the comparison between the growth rates and striation spacings measured on side 1 in the weld metal specimen, W2, as shown in Figure 7.27 (a). The underestimation of crack growth rate is especially evident at the high stress intensities in the welded specimen W3 (Figure 7.27 (b)), and it can be seen that the striation spacing never in fact exceeds 1,2 x 10^{-6} m/cycle. These Figures also indicate that there is no consistent difference between the striation spacings measured near to each side (plane stress) and those measured at mid-thickness where plane strain conditions may exist.

The results obtained for the parent plate specimens are shown in Figure 7.28, and again it can be seen that the striation spacing generally underestimates the crack propagation rate, and that this is again more evident in Figure 7.28 (b) at the higher cyclic stress ranges (65 and 70 MPa $\sqrt{m}$). Unlike the results obtained for weld metal specimens, however, there are instances when the fatigue striation spacing overestimates the macroscopic crack growth, as shown in Figure 7.28 (b). It should be noted here that each of the data points for the striation spacings represent an average of at least two measurements; generally, it was possible to make three separate measurements from each fractograph.

These results would threfore seem to indicate that there is no correlation between striation spacings and macroscopic growth rates. However, when the striation spacing results are plotted against the cyclic stress intensity, as shown in Figure 7.29, there appears to be some agreement between the striation spacings and the scatter band obtained in the macroscopic growth rates. This is most evident for the weld metal specimens (W2 and W3) shown in Figure 7.29 (a), where the striation spacing only underestimates the observed growth rate at ΔK levels in excess of 70 MPa $\sqrt{m}$. This agreement is due to the large range of crack growth rates observed during the testing; it will be recalled that more consistent crack growth rates were achieved in the parent plate specimens, and this is reflected by the fact that fewer striation spacing measurements lie within the (smaller) scatter band in Figure 7.29 (b). This data also illustrates the caution that must be used in comparing data on a log-log plot. Thus, Figure 7.29 (a) suggests that there is mostly good agreement between macroscopic growth rate and striation spacing. Consideration of the corresponding <u>actual</u> data, however, (Figure 7.27) shows clearly that striation spacing and macroscopic growth rate are <u>not</u> consistent, with striation spacing generally underestimating crack growth rate.

These data are summarised in Figure 7.30 which plots the crack growth rate as a function of the striation spacing for all four specimens; and this Figure clearly indicates the trend of underestimation of crack growth rate. As shown in Figure 7.30, a first degree line was best fitted to this data using a multiple regression technique. It will be seen that there is considerably more scatter in these results than those shown in Figure 7.4 (from reference (28)), but it must be pointed out that the degree of scatter in the present results (Figure 7.26) increases with increasing crack growth rate, and there is less data for these higher growth rates in Figure 7.4.

It will be recalled from Section 7.1.3 that Bates and Clark (28) proposed that the striation spacing was a function of the strain in the vicinity of the crack tip. Accordingly, the results obtained in this study were plotted as a function of the applied strain (as defined in equation (7.1)), and the results are shown in Figure 7.31. The results obtained in this study were used as input data to calculate a best fit line using a one degree polynomial regression, and this indicates that, for the material and stress levels used, a more appropriate form of the equation would be:-

$$\text{striation spacing} = 0.2586\ (\triangle K/E)^{2.1} - 1.9 \qquad (7.4)$$

Such a correlation has no physical significance, however, since it infers that the striation spacing negative when there was no strain at the crack tip. (It should be noted here, that this parameter for crack tip strain is analogous, but not exactly equal, to the crack tip opening displacement, or COD.)

Bates and Clark's equation has also been plotted on Figure 7.31, and it can be seen that this corresponds to the finer striations measured in this study. This can be illustrated by considering a crack tip strain of 5×10^{-8}, for example, where the measured striation spacing ranges between 0,2 and 1,2 um, and Bates and Clarke's line can be seen to correspond with the striation spacing of 0,3. There is, however, some considerable scatter in the results, indicating that it may not be possible in practice to estimate crack tip strain (or cyclic stress intensity) from striation spacings.

Finally, it should be pointed out that if the coarse striations underestimate the crack growth rate, the fine striations would represent an even lower crack growth rate, and therefore would have an even poorer correlation with the macroscopic growth rates.

7.4 Summary

This Chapter has detailed the results of a study which attempted to correlate fatigue striation spacings with macroscopic growth rates, and hence estimate the level of applied stress intensity.

The macroscopic growth rates were calculated from optical measurements of crack length extension which was monitored on both sides of the specimens. These results were correlated with those obtained using the potential drop technique for measuring crack length, and it was shown that the potential drop method does indeed account for crack front curvature, thereby providing a total measurement of crack length. The calculated crack growth rates generally showed good agreement; the only exception being the welded specimen (W2) in which uneven crack growth occurred.

Some scatter was observed in the constant ΔK tests, and this was ascribed to errors in crack length measurement; the results obtained, however, were adequate for the purpose of this study.

The fractographic examination revealed that although fatigue occurred by ductile striated growth, the striations were not always well defined, and tended to occur in packets. Both fine and coarse striations were found in close proximity to each other, and in some instances the fine striations were seen to be sub-units of the coarse striations. The coarse striations' spacings were seen to be more representative of the observed crack propagation rates, and thus these were used in the correlation reported here. At high levels of applied stress intensity, the striations were separated by areas of ductile void coalesence. However, the fractographic study did locate areas of well defined ductile striated growth, both in the weld metal and in the parent plate.

The correlation of striation spacings with macroscopic growth rates indicated that the striations tended, on the whole, to underestimate the true crack propagation rate, and this was particularly evident at the higher stress intensities (i.e. greater than 65 MPa $\sqrt{m}$). The overall correlation of striation spacing with macroscopic growth rate was very poor; however there was an apparently good correlation with the scatterband of the measured macroscopic growth rates when the striation spacings were plotted against ΔK in the normal log-log fashion. In the case of the weld metal specimens, the striation spacings fell within the scatter band of the macroscopic growth rates up to a cyclic stress intensity of 70 MPa $\sqrt{m}$. There was less correlation in the case of the parent plate specimens, due to the fact that the scatter band for the macroscopic growth rates calculated for these specimens was smaller than that for the weld metal specimens. This therefore indicates that some circumspection must be used when comparing striation spacings and macroscopic growth rates with the cyclic stress intensity on a log-log plot. Thus, the reality of the situation may only be made clear when the striation spacing measurements are linearly plotted against the macroscopic growth rates.

At the high growth rates (greater than 2 x10^{-6} m/cycle), the striations were poorly defined, and interspersed between areas of ductile void coalesence. Thus this "static mode" of fracture would contribute to the observed rate of crack propagation, and the striation spacing could not be expected to compare favourably with the corresponding optical or potential drop measurements.

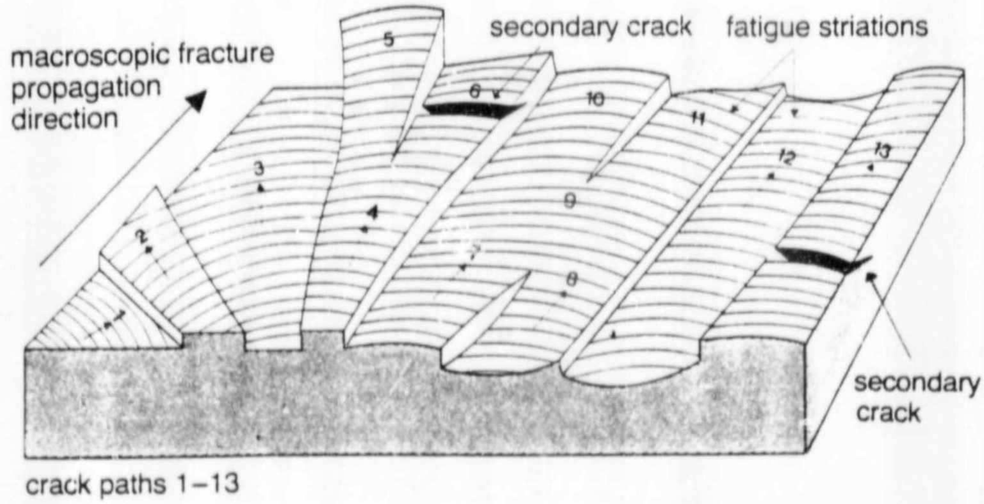

Figure 7.1 An illustration of the different crack paths (1-13) that divide the crack front in polycrystalline materials. (From 133).

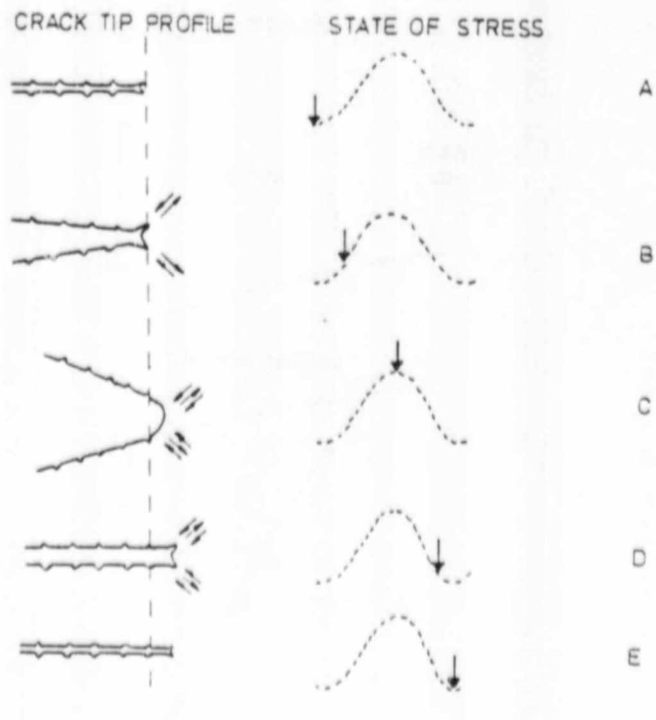

Figure 7.2 Proposed mechanism for (Stage II) fatigue crack propagation and formation of ductile striations (after Laird (135)). (A) unstressed, (B) small tensile stress, (C) peak tensile stress (D) small compressive stress and (E) unstressed.

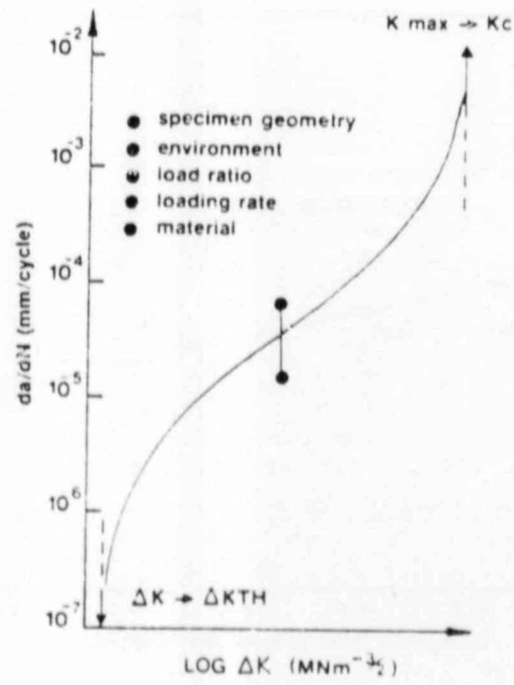

<u>Figure 7.3</u> Typical sigmoidal form of the da/dN versus ΔK curve obtained on a log-log scale (from 1). Note the factors that can affect the crack growth rates.

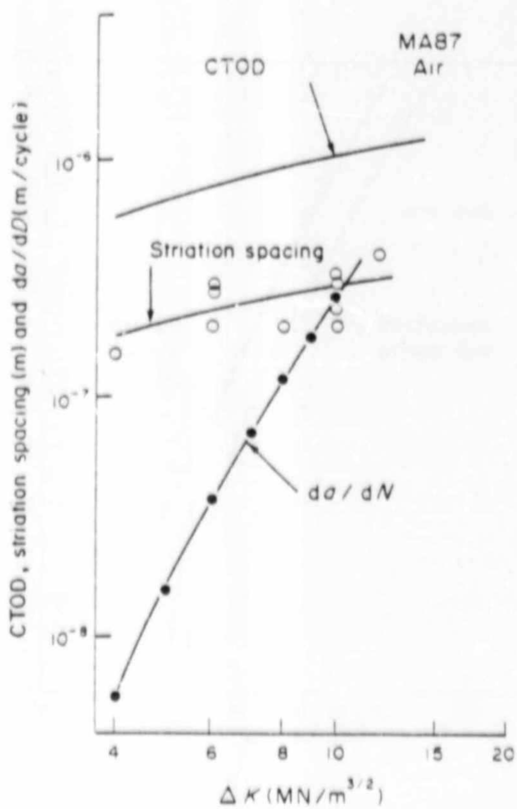

<u>Figure 7.4</u> Comparison of fatigue striation spacing and crack growth rate for an aluminium alloy (from 28).

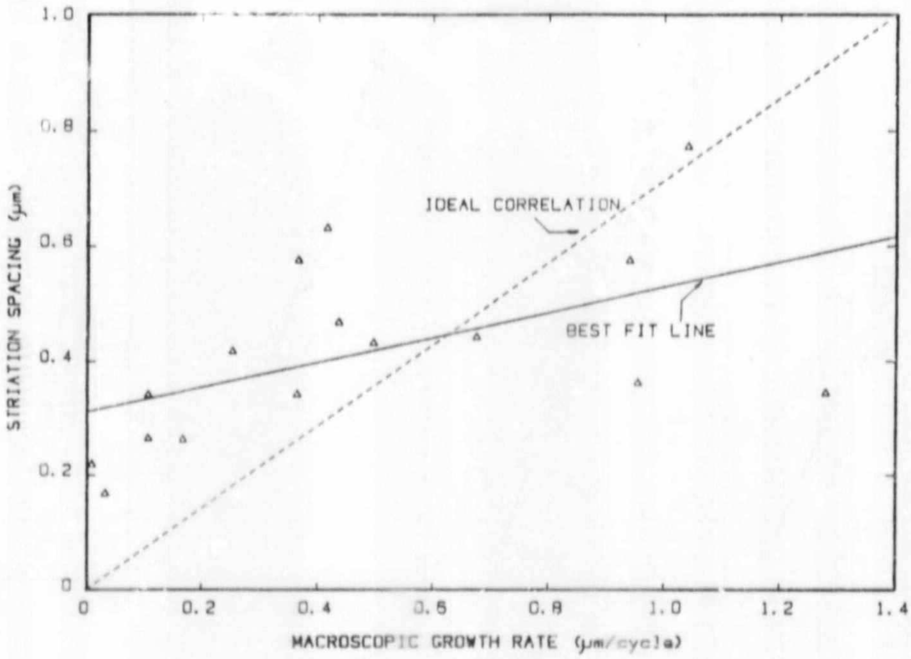

Figure 7.5 Data obtained in the fractographic examination of mild steel specimens, indicating that striation spacings overestimate low growth rates, but underestimate high growth rates (from 26).

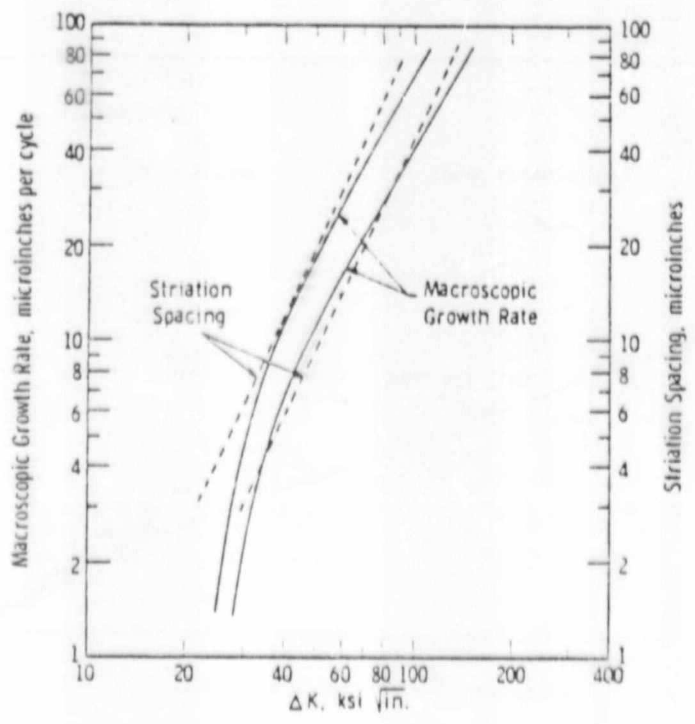

Figure 7.6(a) Comparison of macroscopic crack growth rates and striation spacing for A533 steel (from 25).

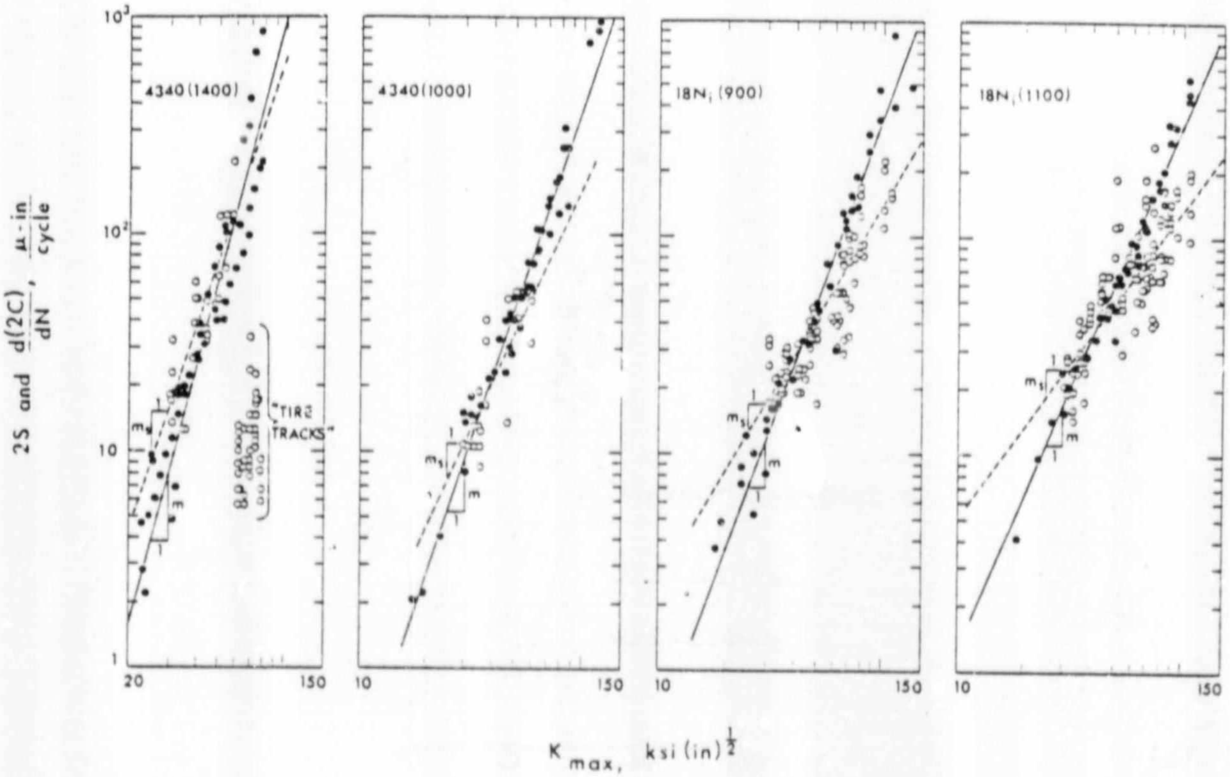

<u>Figure 7.6(b)</u> Comparison of macroscopic growth rate (solid circles and solid line) and fatigue striation spacings (open circles and dotted line) for various high strength steels (after Miller (137)).

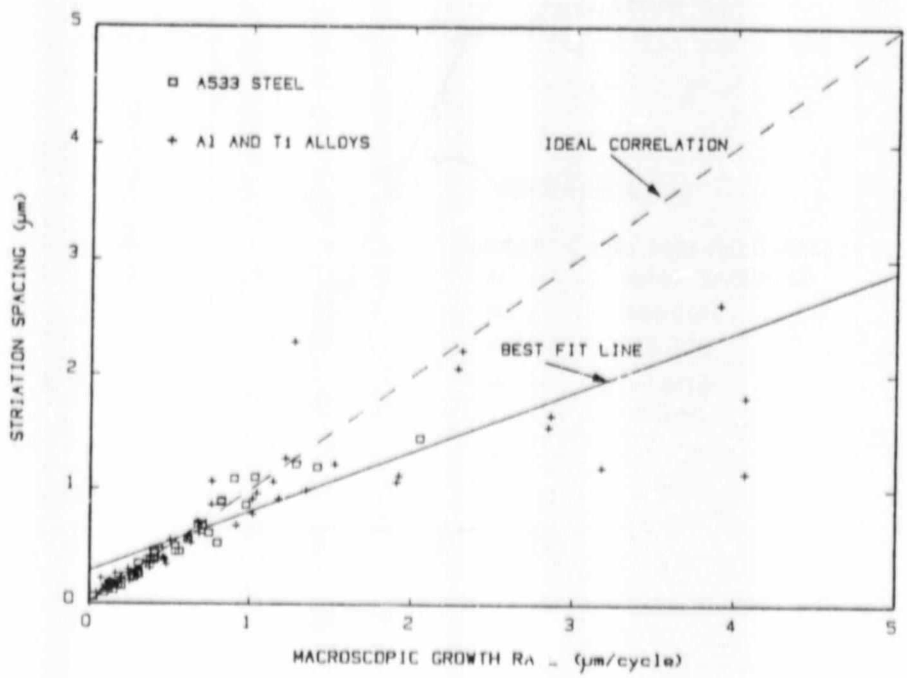

<u>Figure 7.7</u> The variation in fatigue striation spacing with crack propagation rate obtained by Bates and Clark (28). Note the deviation from the ideal correlation at high growth rates.

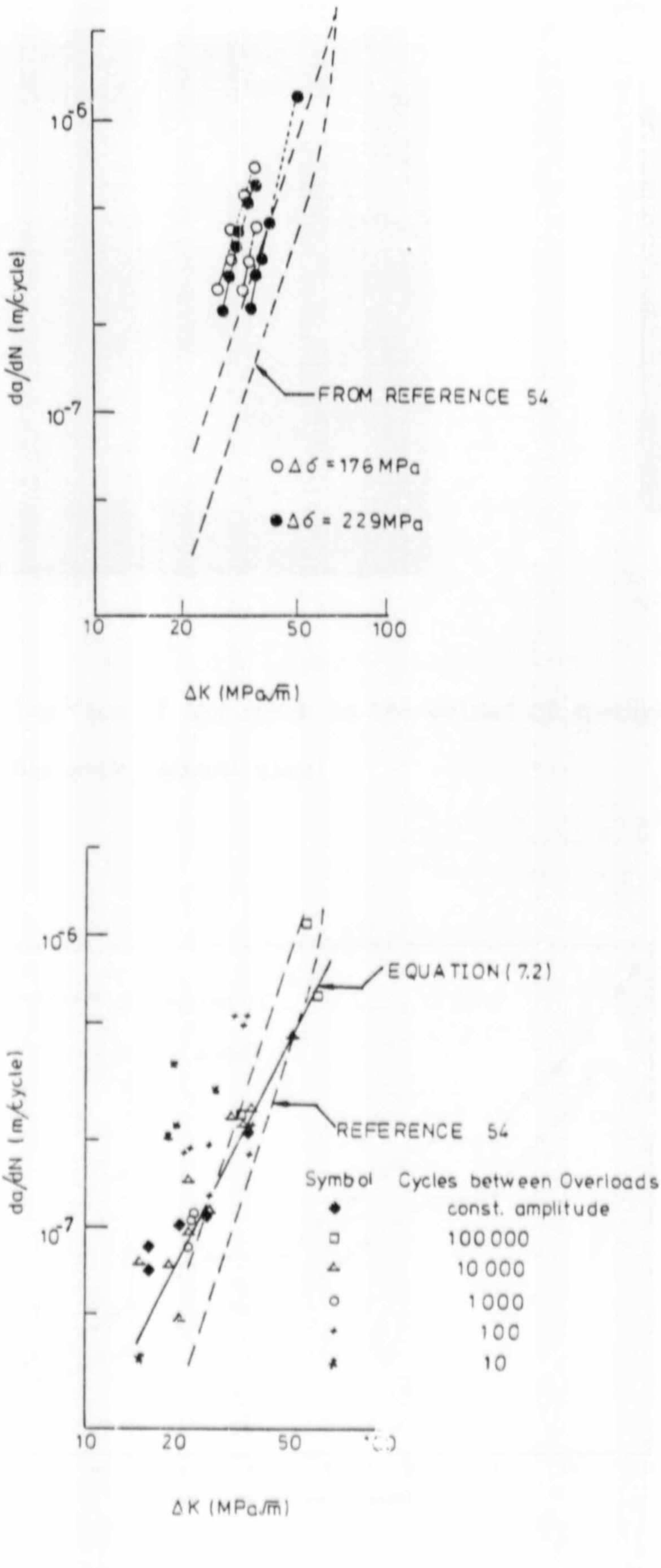

(a)

(b)

<u>Figure 7.8</u> The correlation between (a) "macroscopic" striation spacings and (b) microscopic striation spacings and the crack growth rates obtained from the literature (from 27).

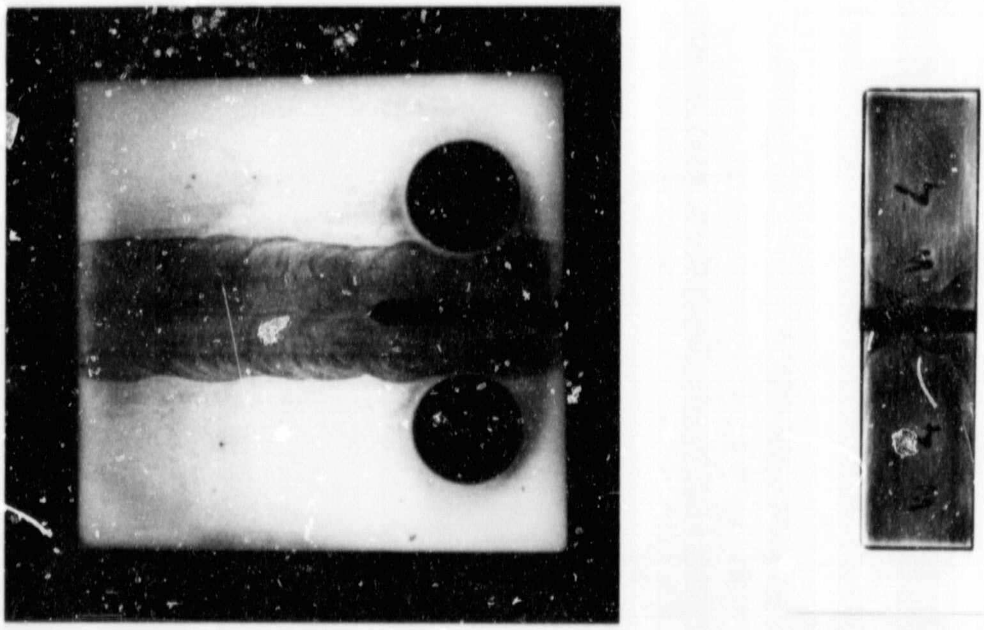

<u>Figure 7.9</u> The location of the notch in the welded CT specimen used in this work (actual size).

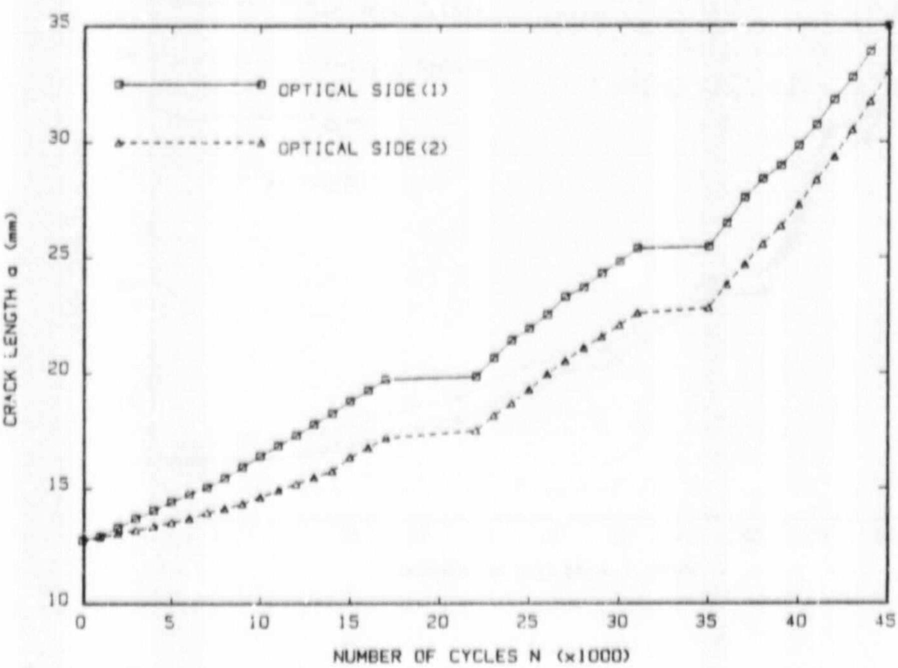

<u>Figure 7.10</u> The change in crack length with number of loading cycles as measured on the two sides of specimen W2.

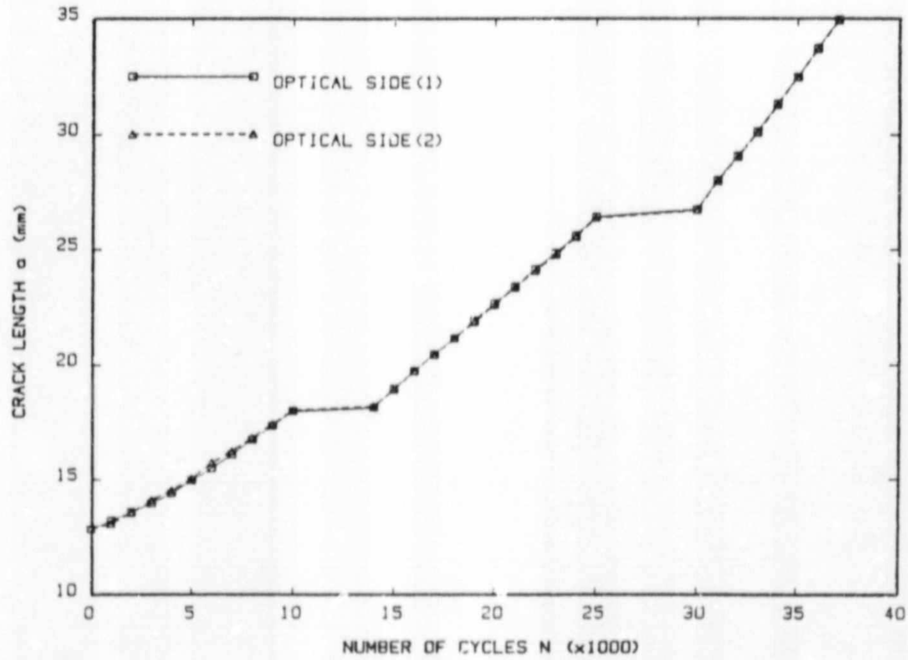

<u>Figure 7.11</u> The change in crack length with loading cycles for the parent plate specimen P4. Note the good agreement in the two sets of measurements.

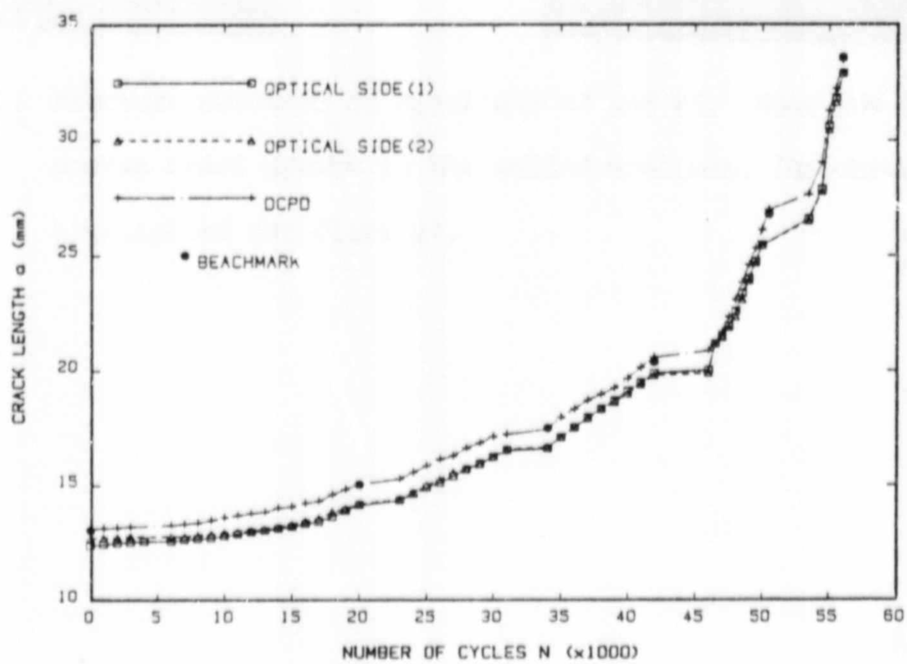

<u>Figure 7.12</u> The change in crack length with loading cycles for specimen W3, as measured optically, and using the potential drop. Note that the potential drop coincides with the average length of the beachmarks, thus accounting for crack curvature.

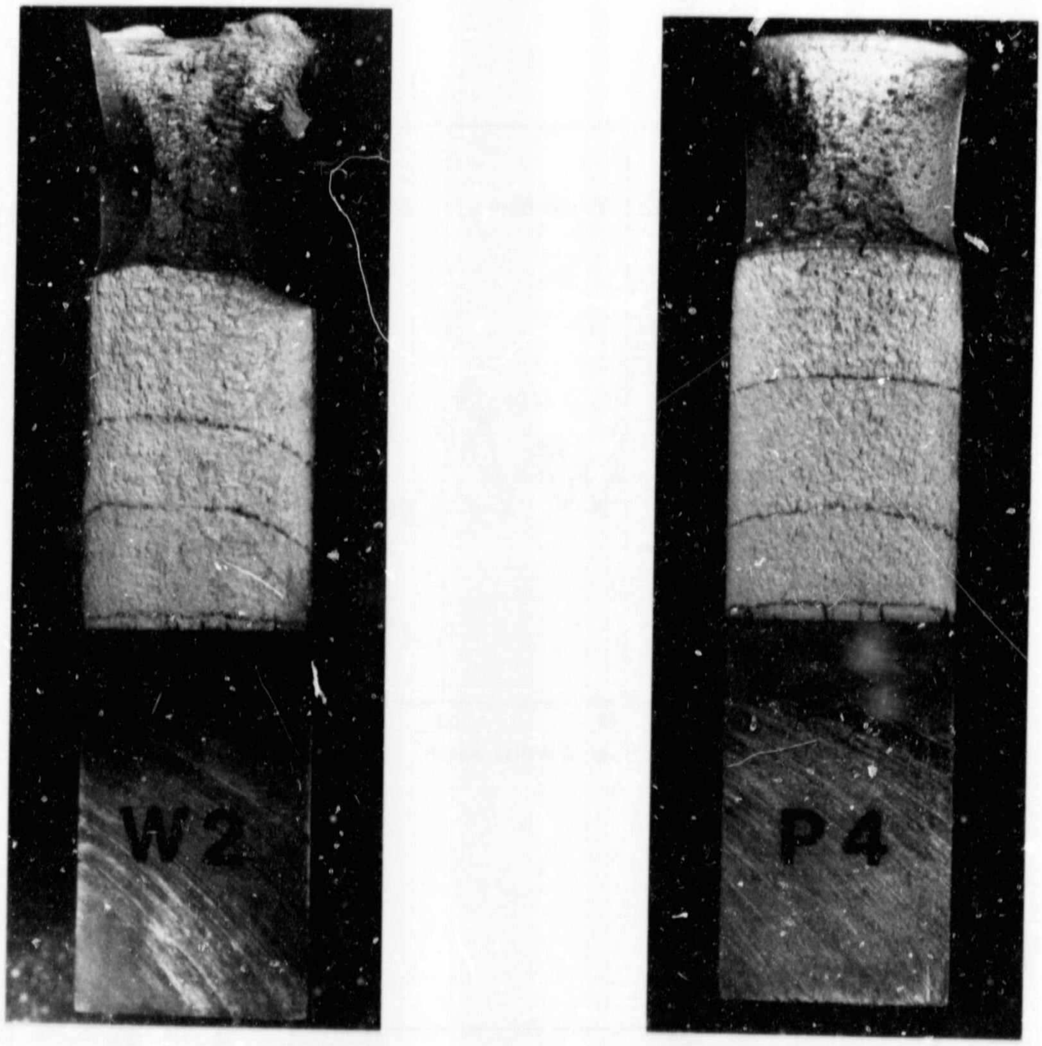

Figure 7.13 Fracture surfaces of specimens W2 and P4. Note the uneven crack growth in the welded specimen. (Beachmarks highlighted for clarity).

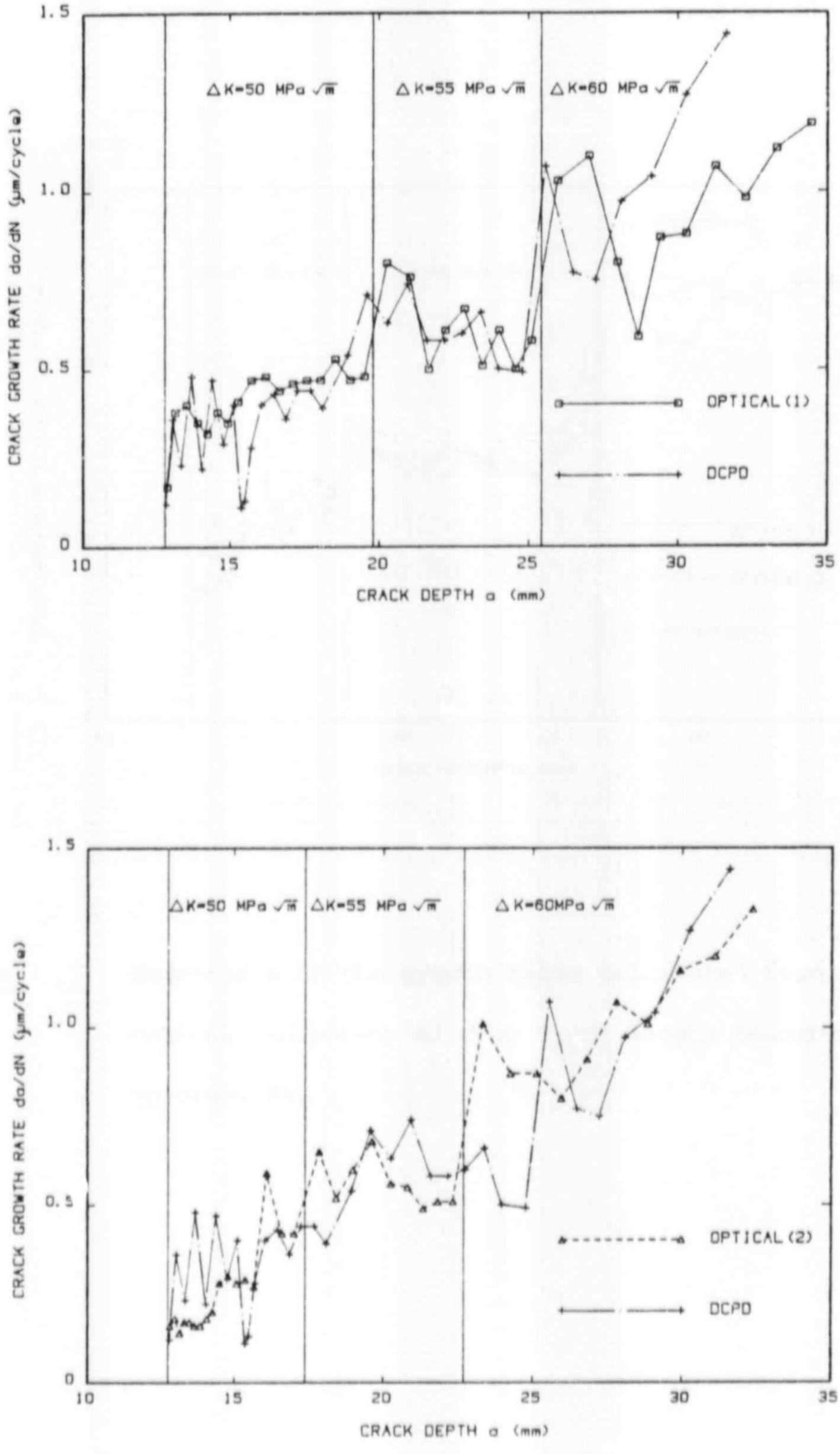

(a)

(b)

<u>Figure 7.14</u> Comparison of macroscopic growth rates evalulated from the potential drop to that calculated from the optical measurements made on (a) side 1, and (b) side 2 for specimen W2.

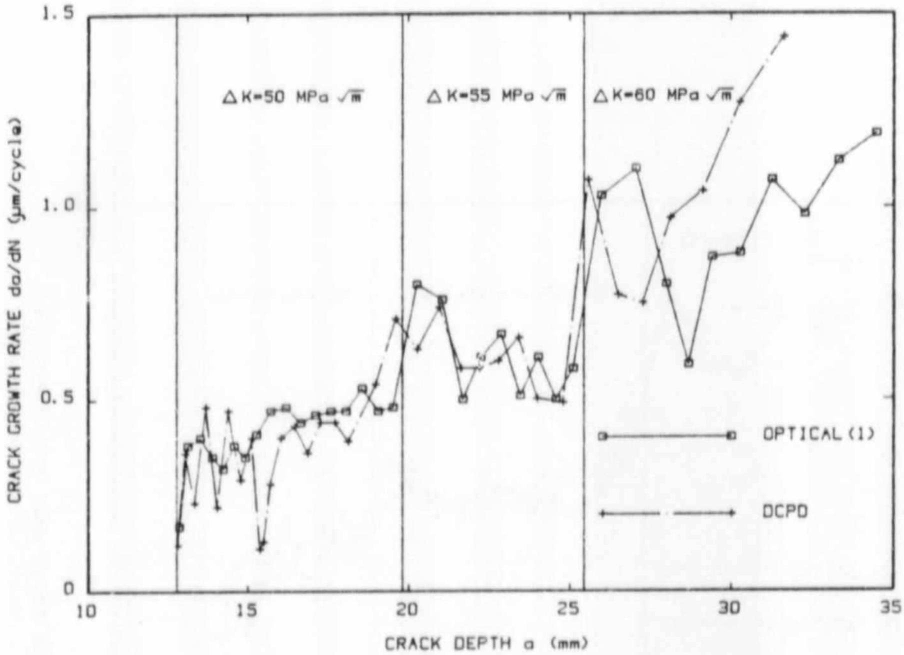

(a)

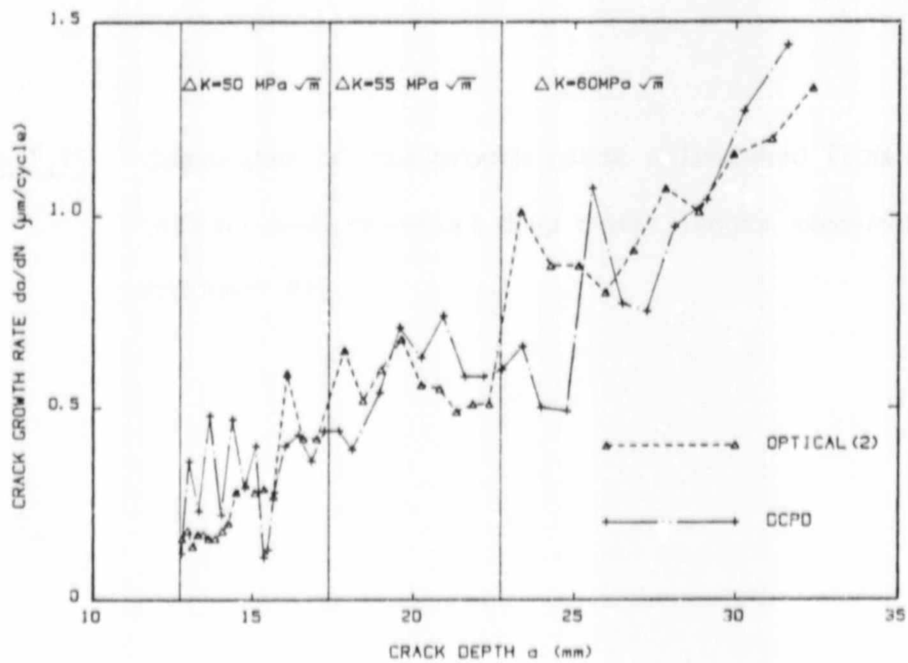

(b)

Figure 7.14 Comparison of macroscopic growth rates evalulated from the potential drop to that calculated from the optical measurements made on (a) side 1, and (b) side 2 for specimen W2.

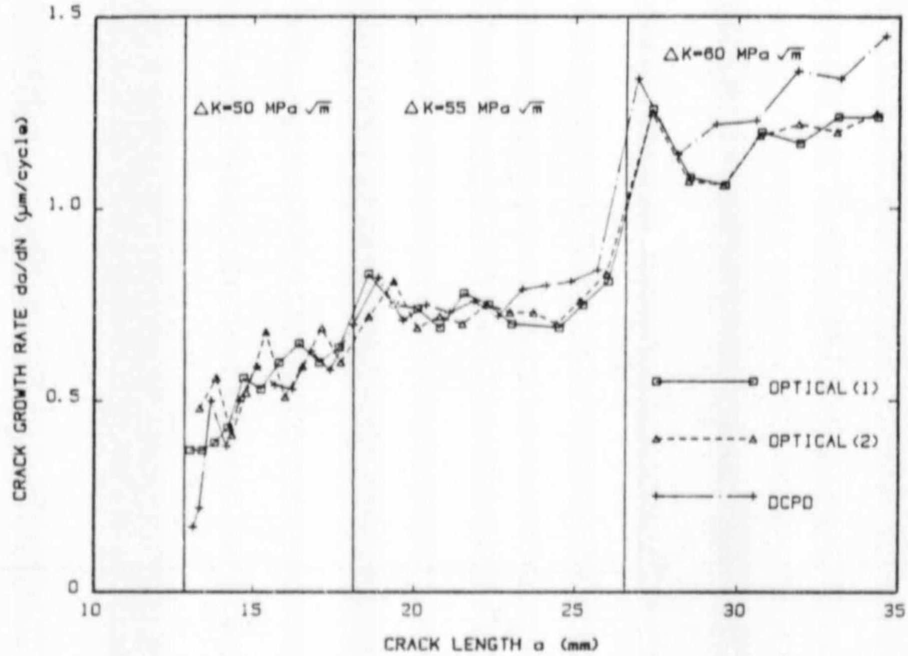

Figure 7.15 Comparison of the growth rates calculated from the optical and potential drop crack length measurements in specimen P4.

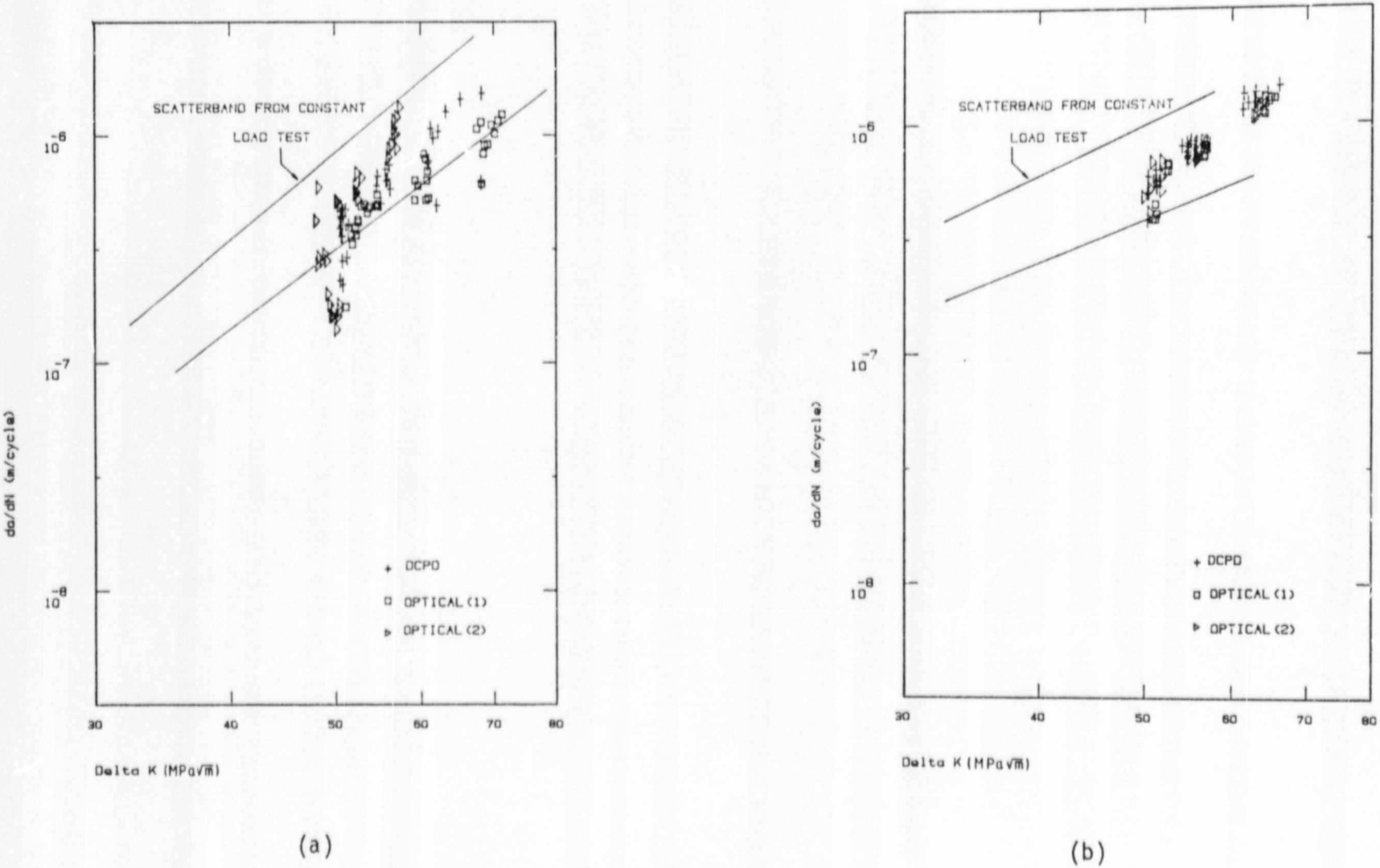

<u>Figure 7.16</u> Crack propagation rate versus cyclic stress intensity for (a) specimen W2 and (b) specimen P4. Note the reduced scatter obtained in the parent plate specimen (the solid lines indicate the results of the preliminary constant load tests).

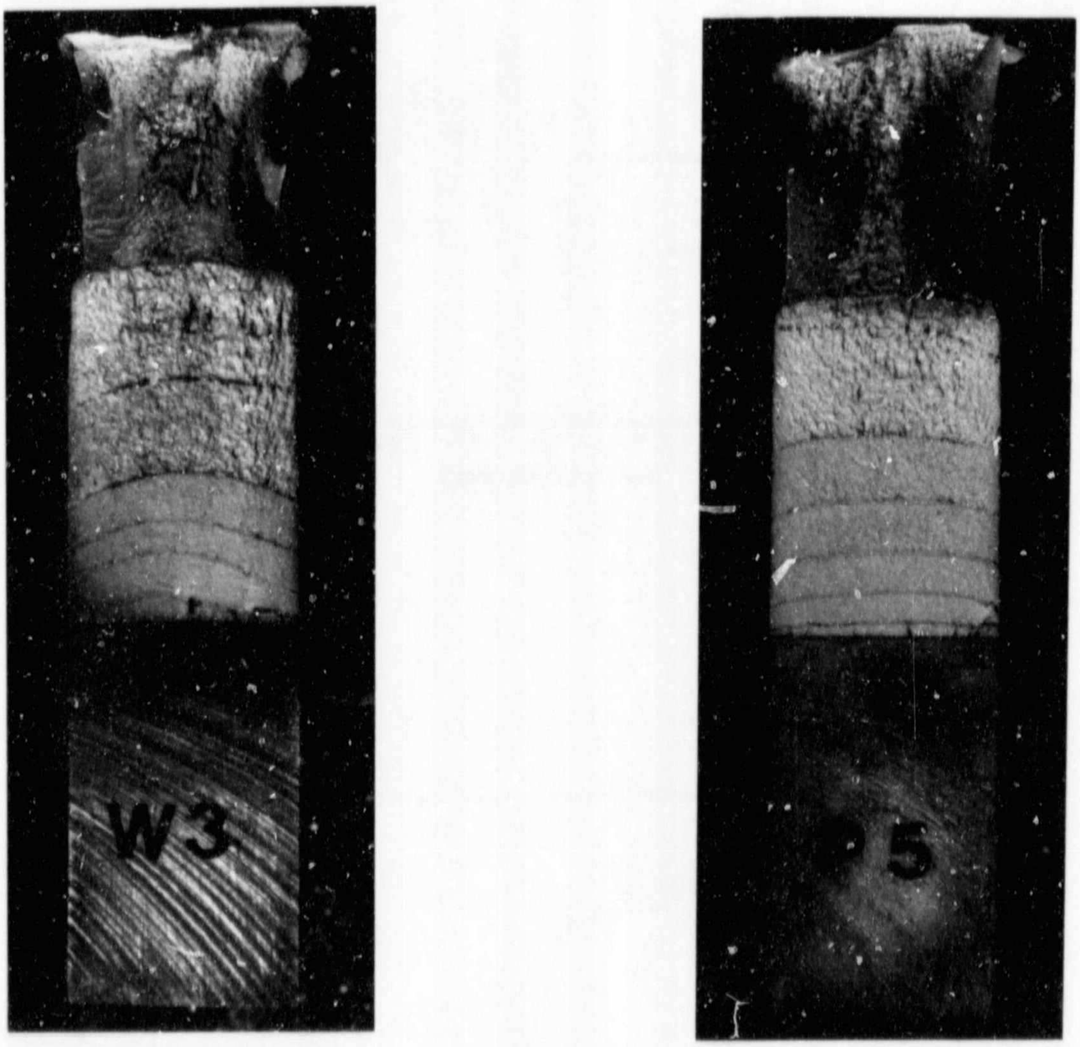

Figure 7.17 Fracture surfaces of specimens W3 and P5. Note that the crack curvature in W3 decreases with crack length.

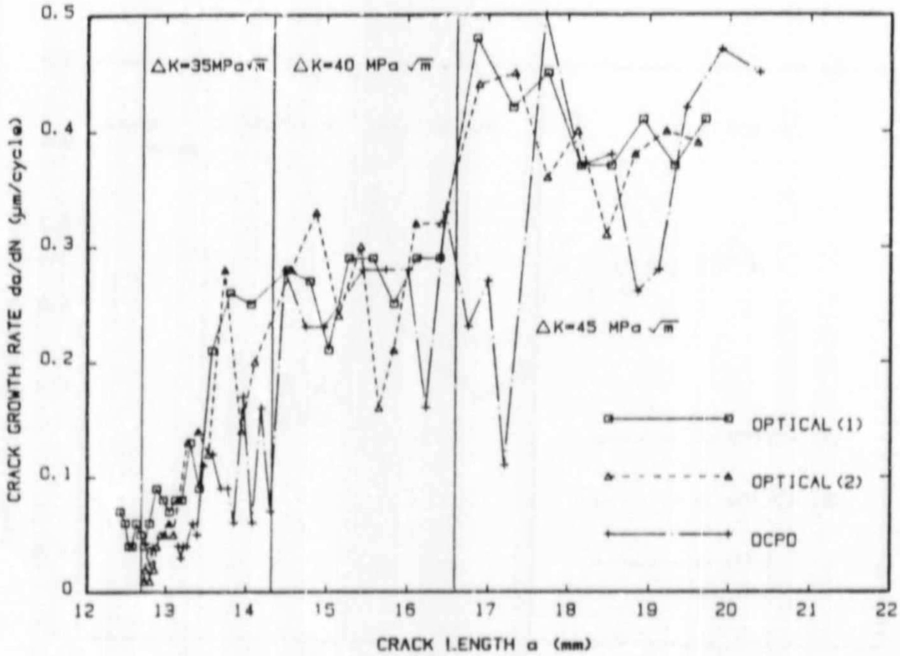

(a)

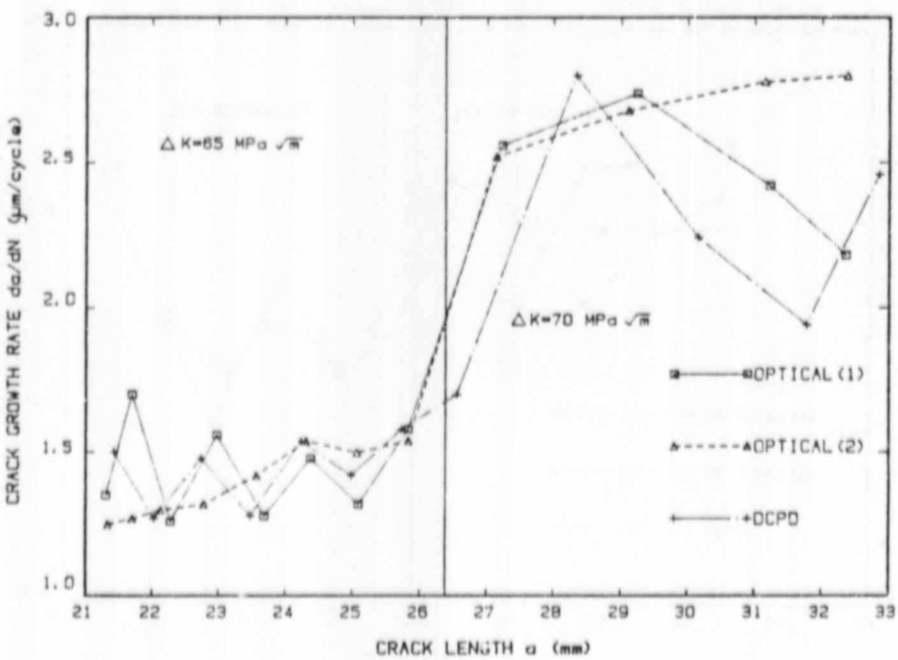

(b)

<u>Figure 7.18</u> Fatigue crack growth rates evaluated for specimen W3 at nominal stress intensities of (a) 30,35,40 and 40 MPa $\sqrt{m}$ and (b) 65 and 70 MPa $\sqrt{m}$.

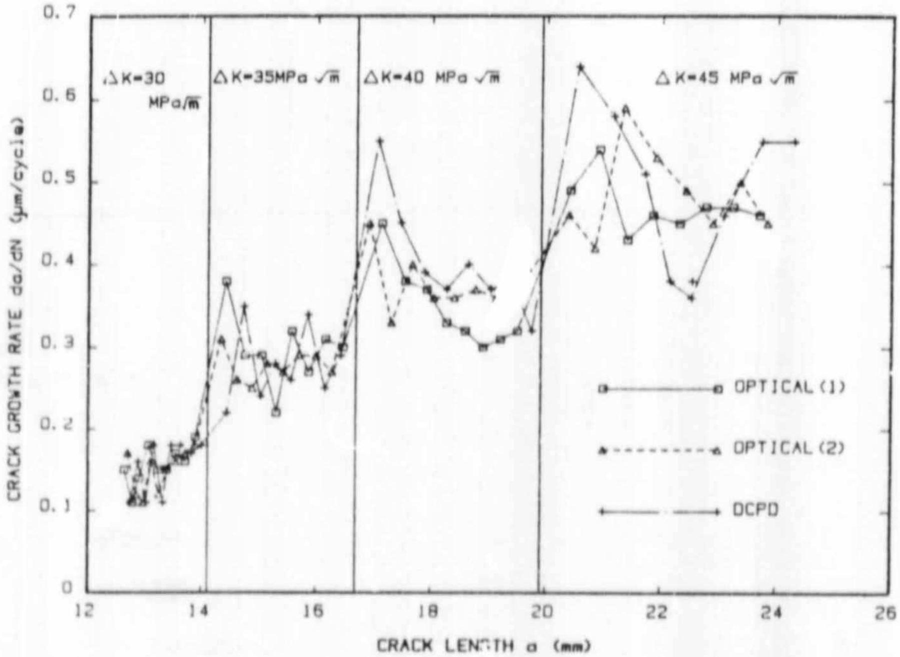

(a)

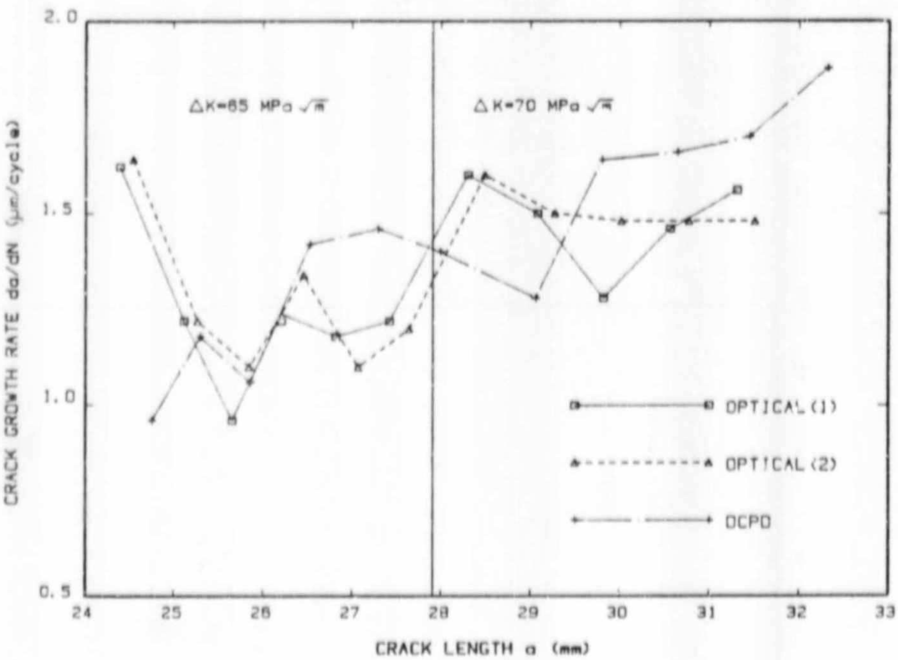

(b)

<u>Figure 7.19</u> The fatigue crack growth rates as measured in specimen P5 at nominally constant $\triangle$K values of (a) 30, 35, 40 and 45 MPa $\sqrt{m}$ and (b) 65 and 70 MPa $\sqrt{m}$.

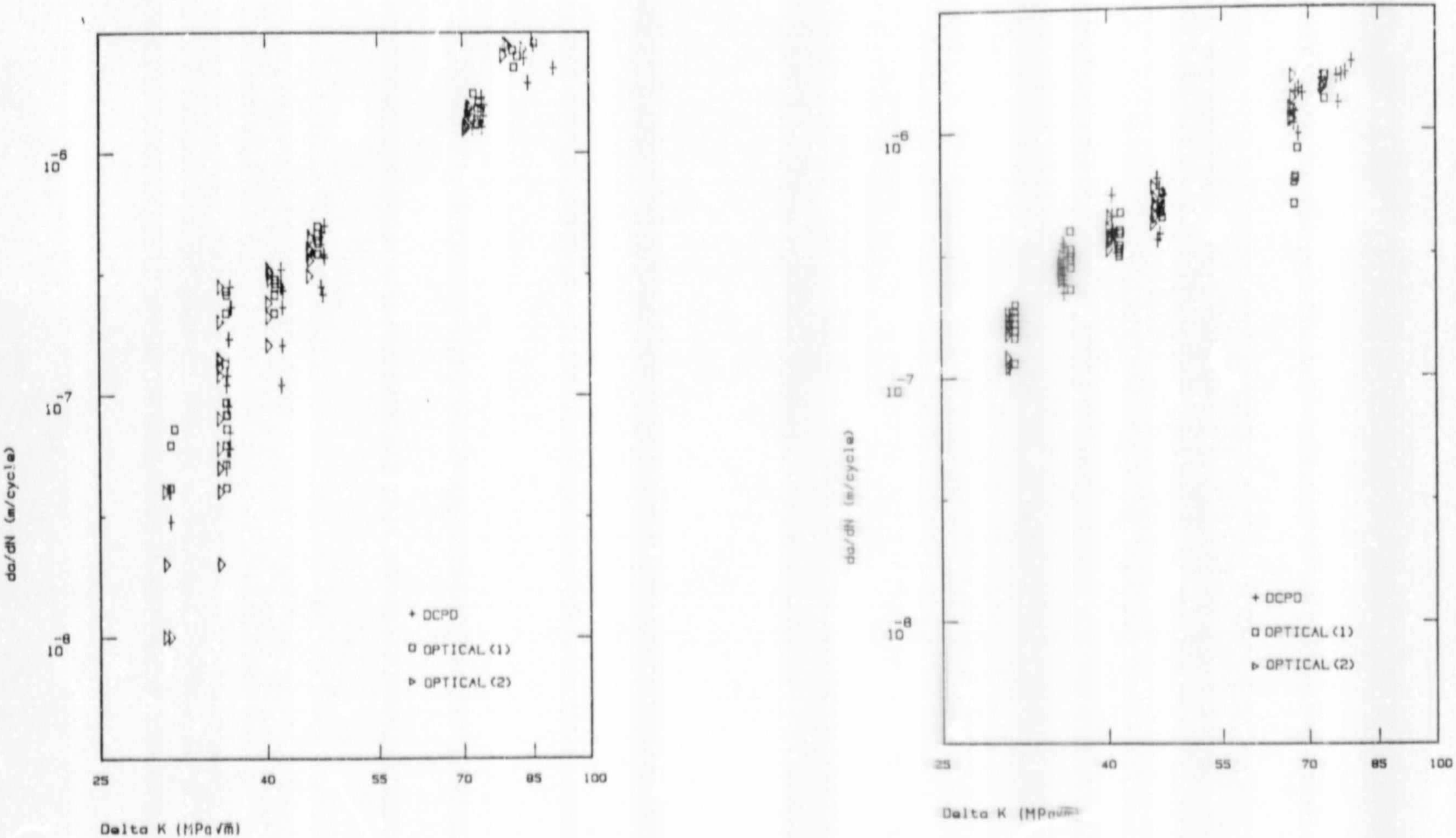

(a) (b)

Figure 7.20 da/dN versus ΔK for specimens (a) W3 and (b) P5. Note that in both graphs, the different ΔK values are easily distinguished.

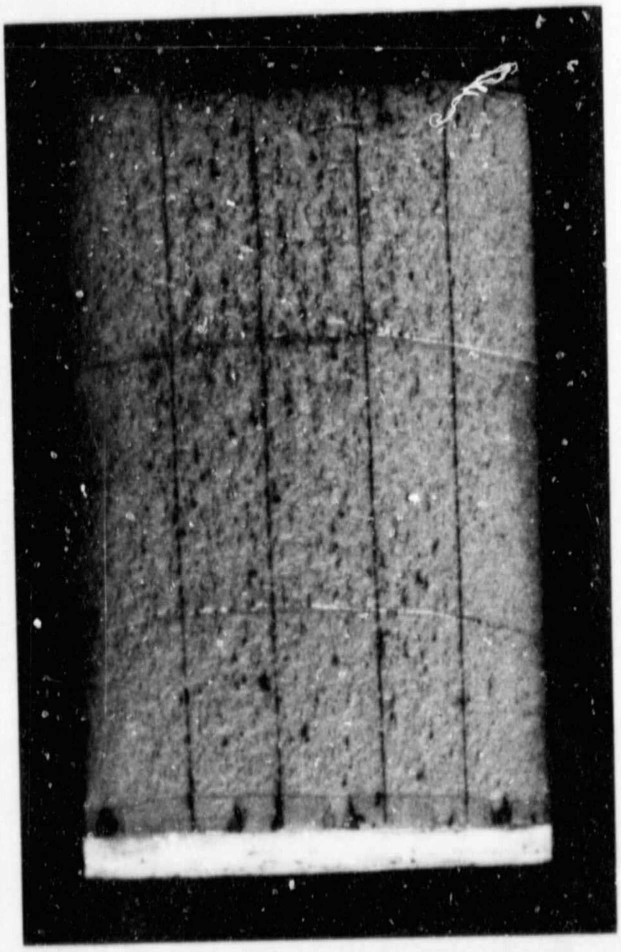

Figure 7.21 The appearance of the specimens used in the SEM work. Note the grid used for easy identification of location of the regions studied at high magnifications.

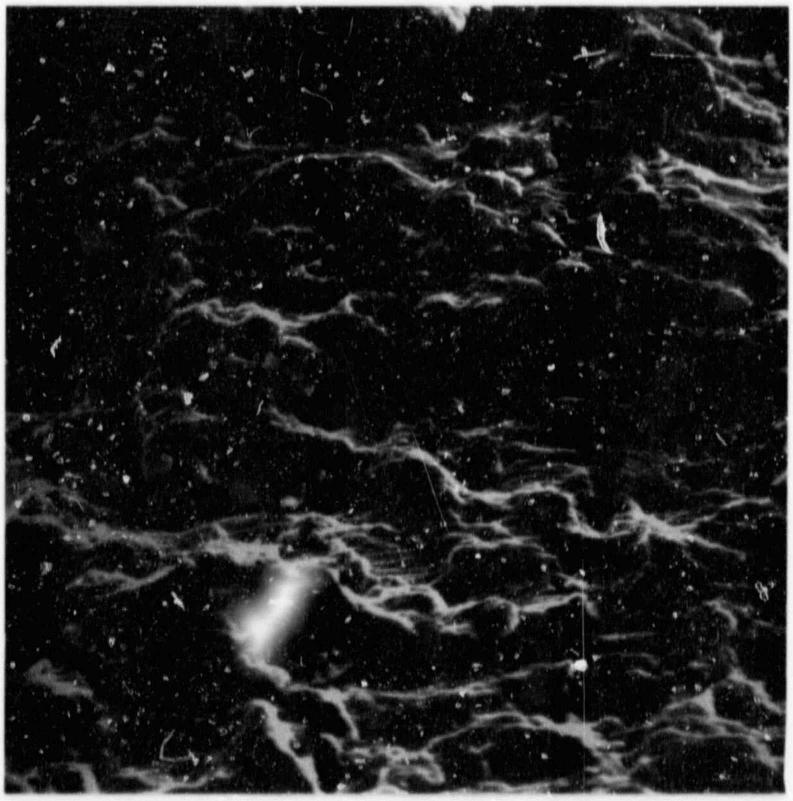

5 μm

(a)

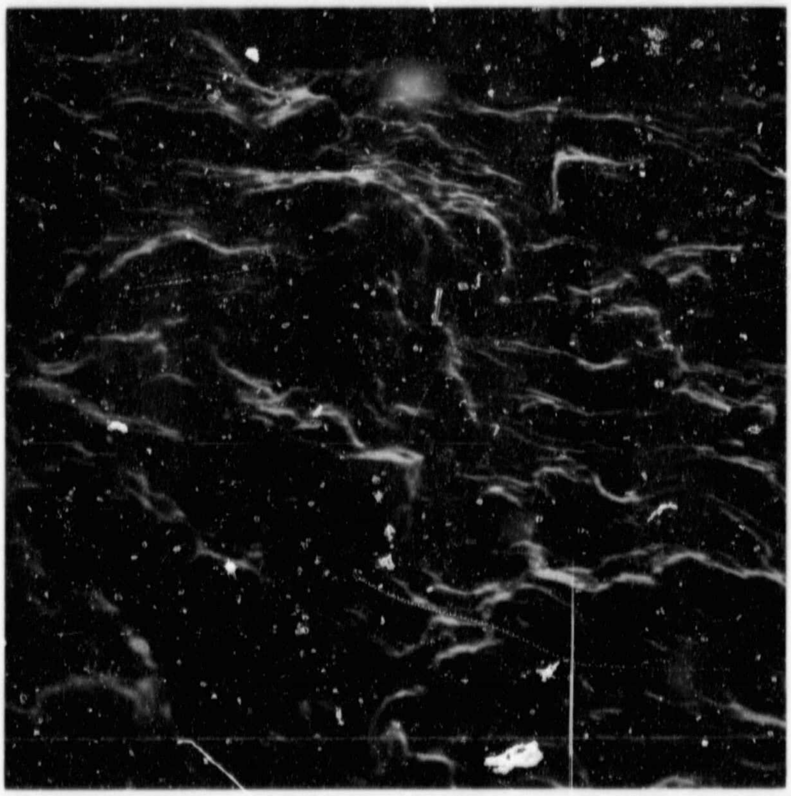

5 μm

(b)

Figure 7.22 Scanning electron fractographs showing how the striations tended to occur in separate "packets" (a) specimen P4 at a ΔK of 55 MPa$\sqrt{m}$, magnification 1680x and (b) specimen P5 at a ΔK of 65 MPa$\sqrt{m}$, magnification 1670x. (In all the fractographic work shown here the specimens are tilted at an angle of 40^{o} towards the detector, and the crack growth direction is towards the top of the page).

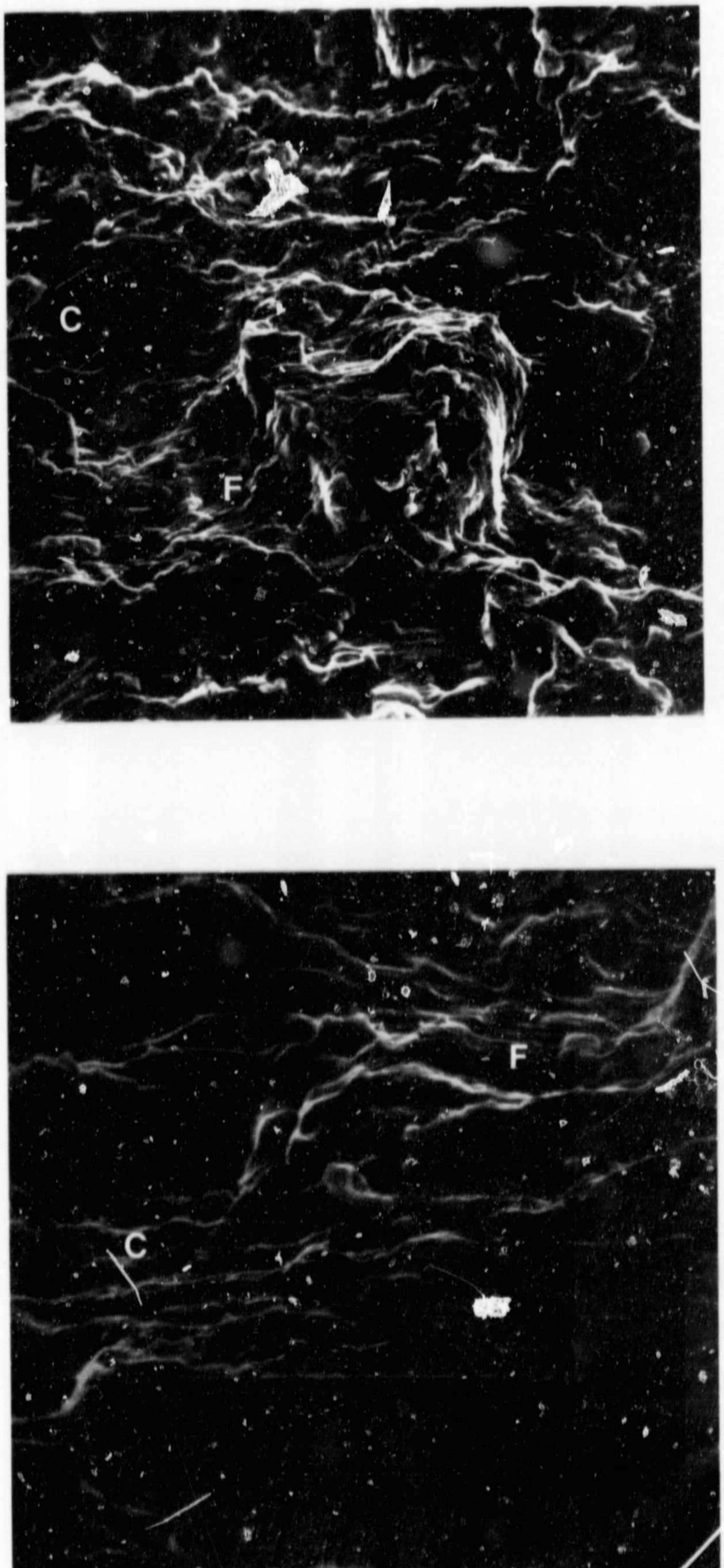

Figure 7.23 The occurrence of coarse (C) and fine (F) striations within close proximity in (a) specimen W a ΔK of 60 MPa $\sqrt{m}$, and 1680x magnification and (b) specimen W3 at a ΔK of 80 MPa $\sqrt{m}$, at 4100x magnification.

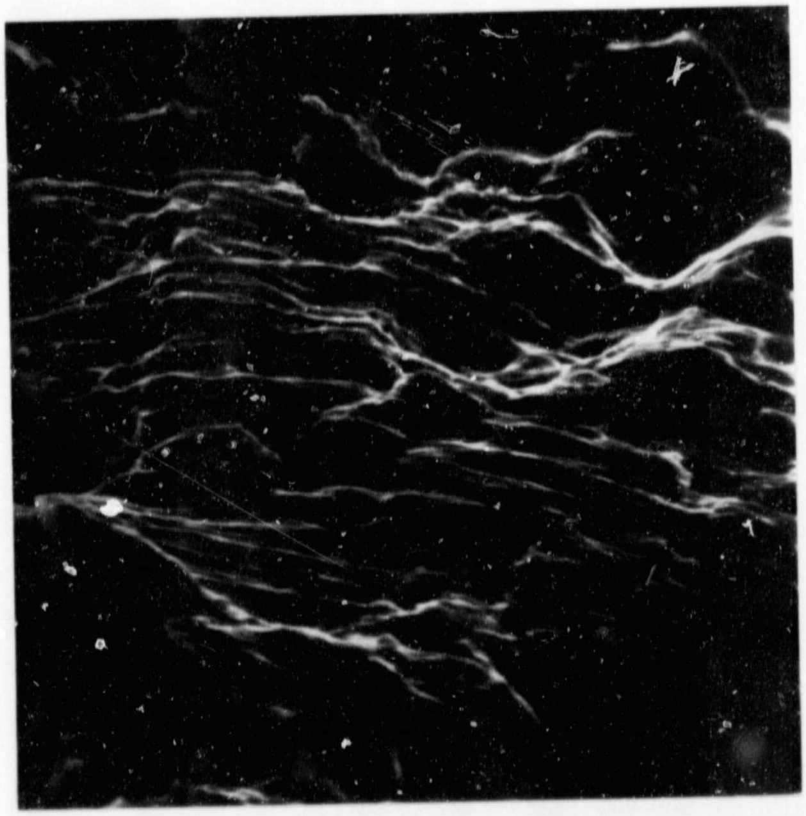

2 µm

(a)

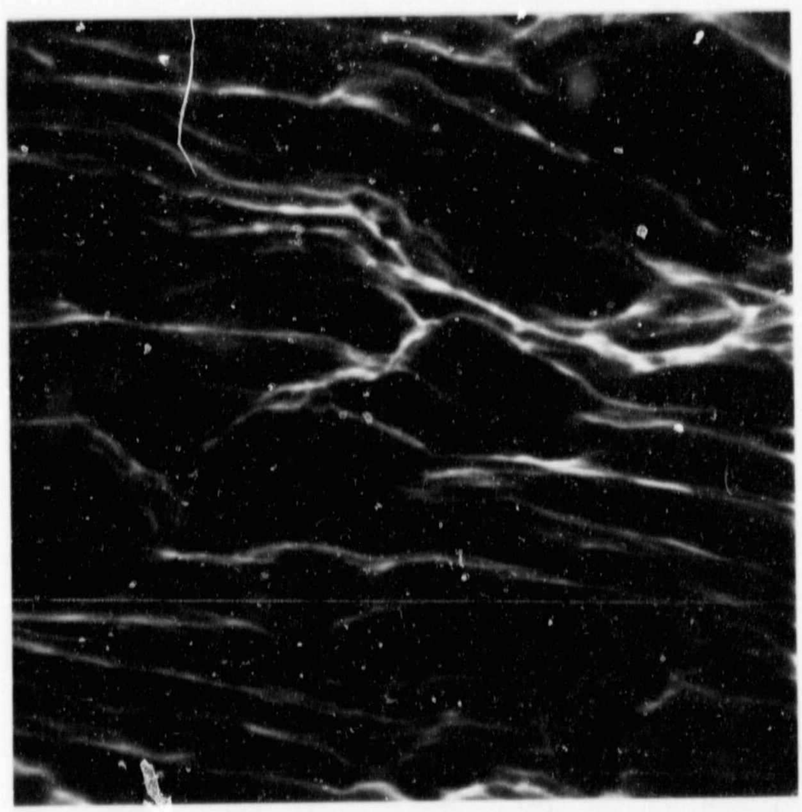

1 µm

(b)

Figure 7.24 Examples of fine striations which appeared to be sub-units of coarse striations. These fractographs were taken from specimen W2 at a ΔK of 50 MPa $\sqrt{m}$ (a) magnification 3675x and (b) same area at a magnification of 7350x.

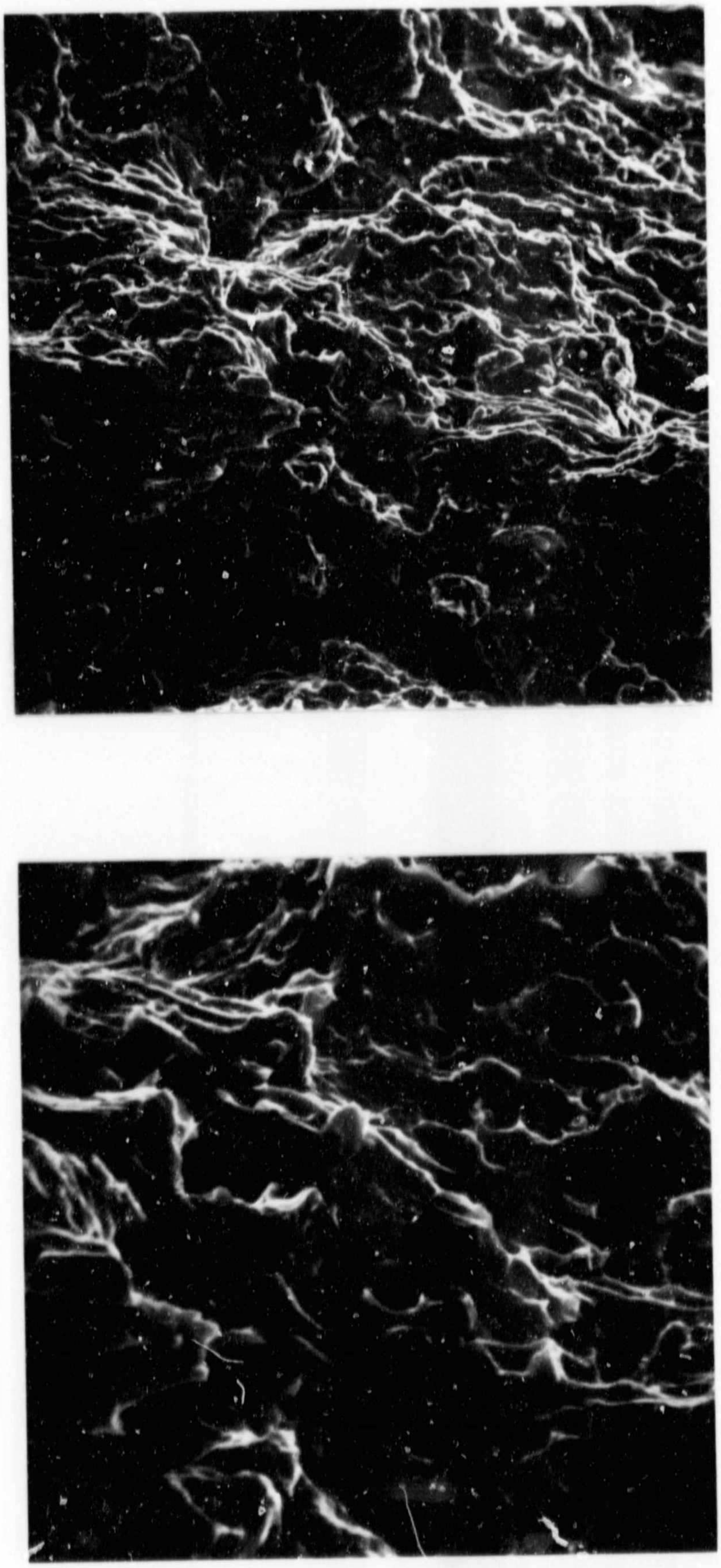

<u>Figure 7.25</u> The appearance of the fatigue-fracture surface in specimen P5 at a ΔK of 70 MPa $\sqrt{m}$. Note that the areas between the striations is fully ductile. (a) 1554x, (b) 3830x.

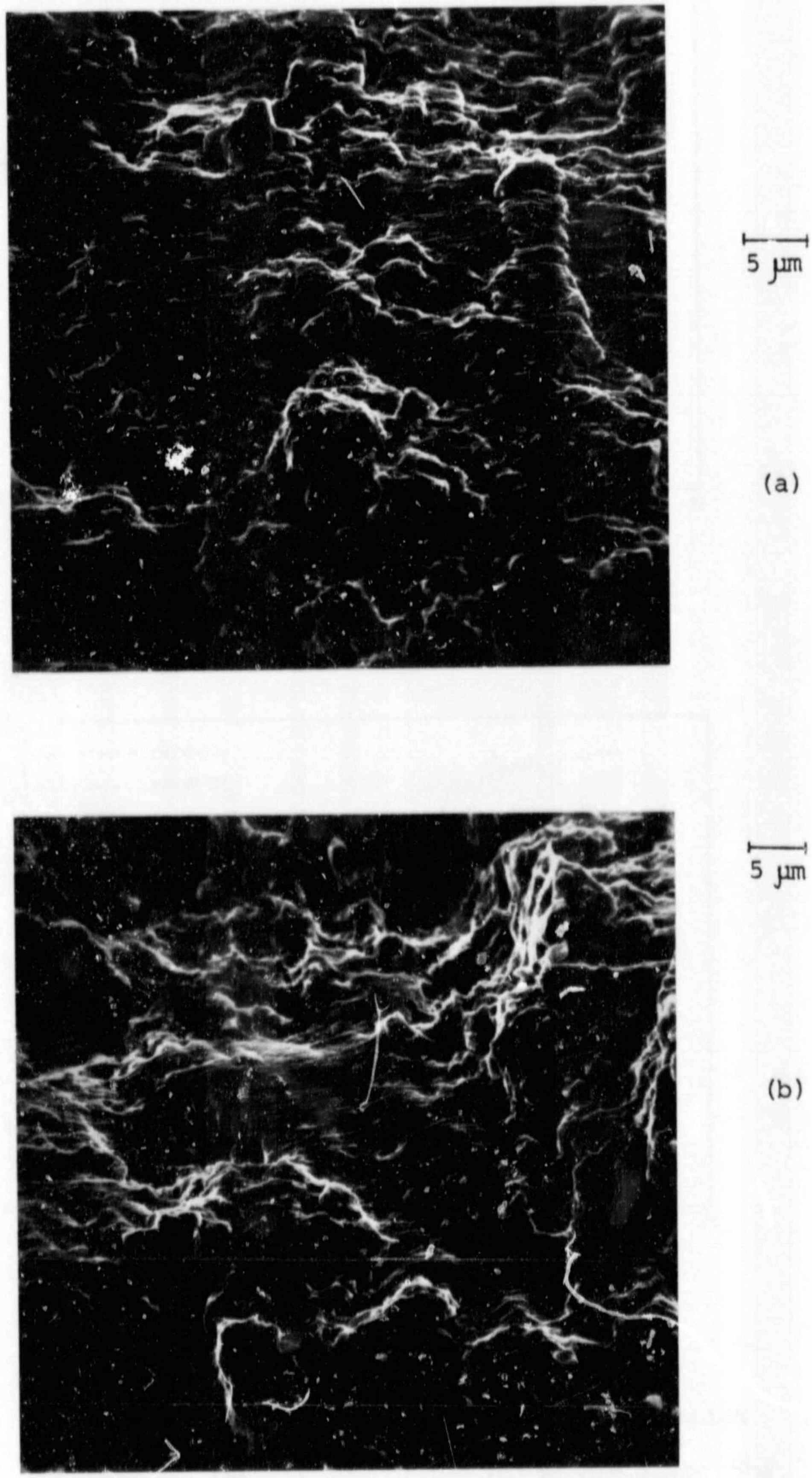

<u>Figure 7.26</u> Well-defined ductile striations in the weld metal specimen W2 at (a) a ΔK of 50 MPa $\sqrt{m}$, magnification 1910x and (b) at a ΔK of 55 MPa $\sqrt{m}$ and 1730x magnification.

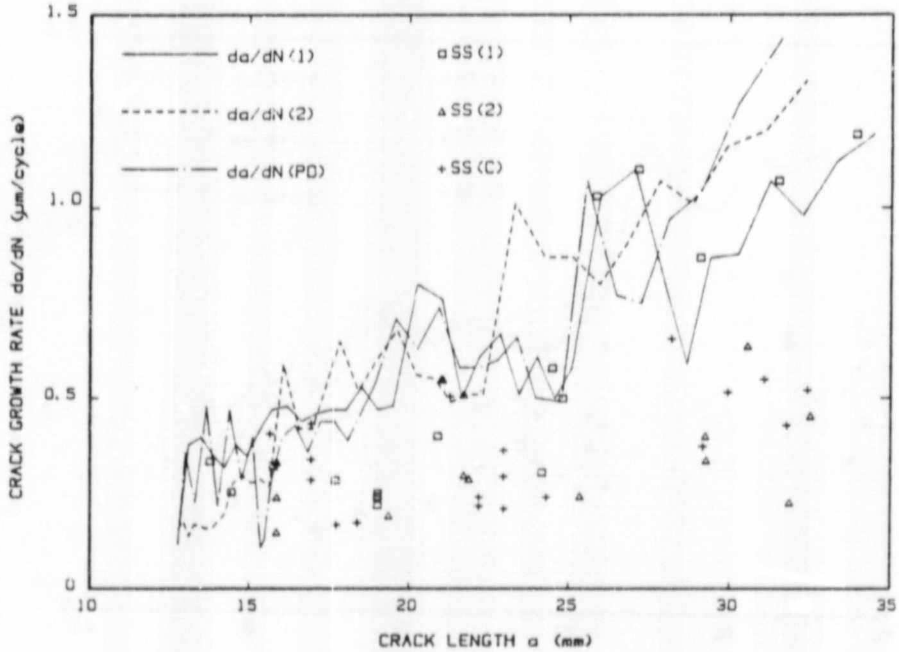

(a)

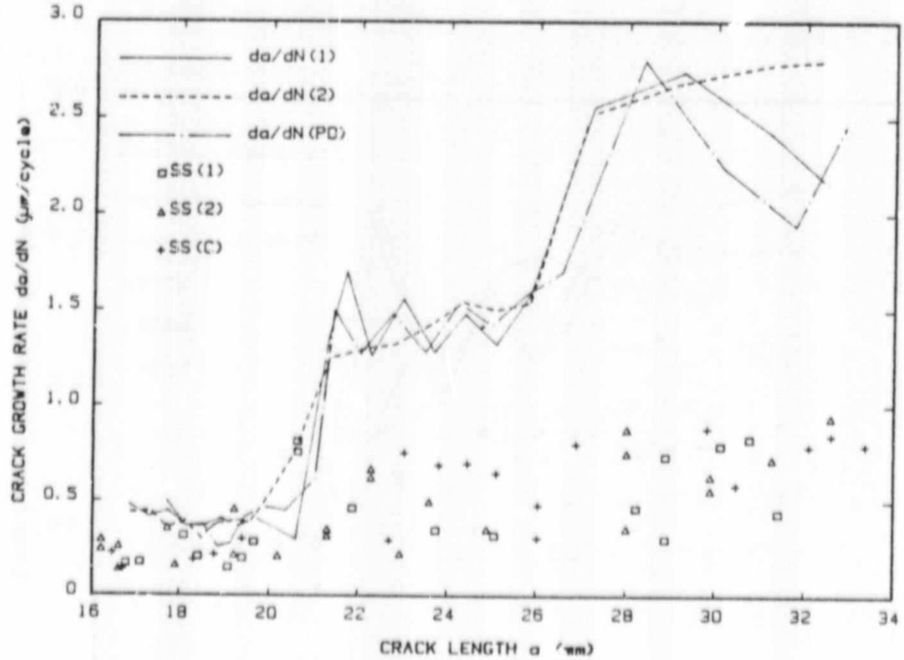

(b)

Figure 7.27 Comparison of macroscopic growth rates and striation spacings for (a) specimen W2 and (b) specimen W3. The different symbols used refer to the location of the microscopic measurements, 1 and 2 denote the sides of the specimen, and C the centre or mid-thickness.

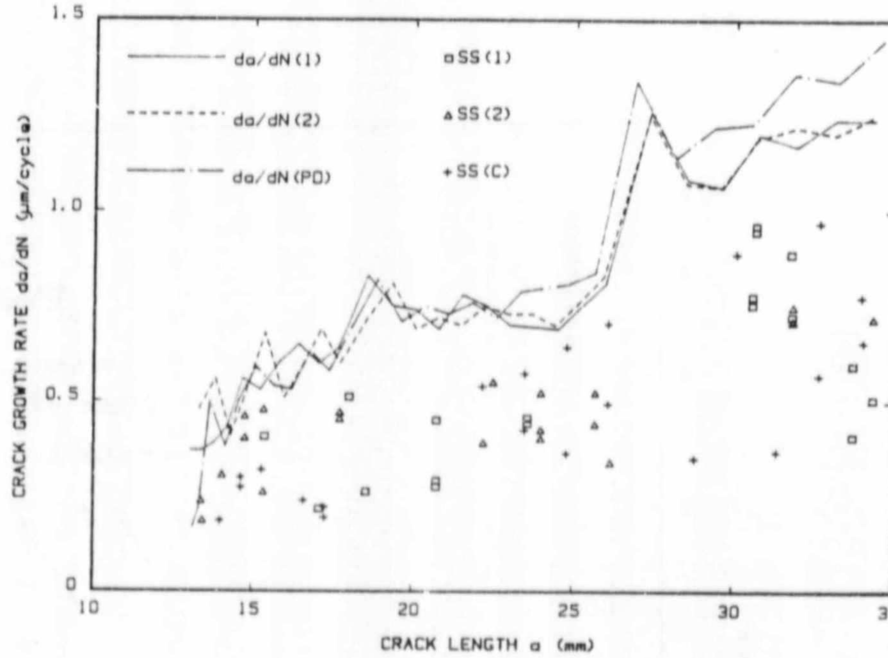

(a)

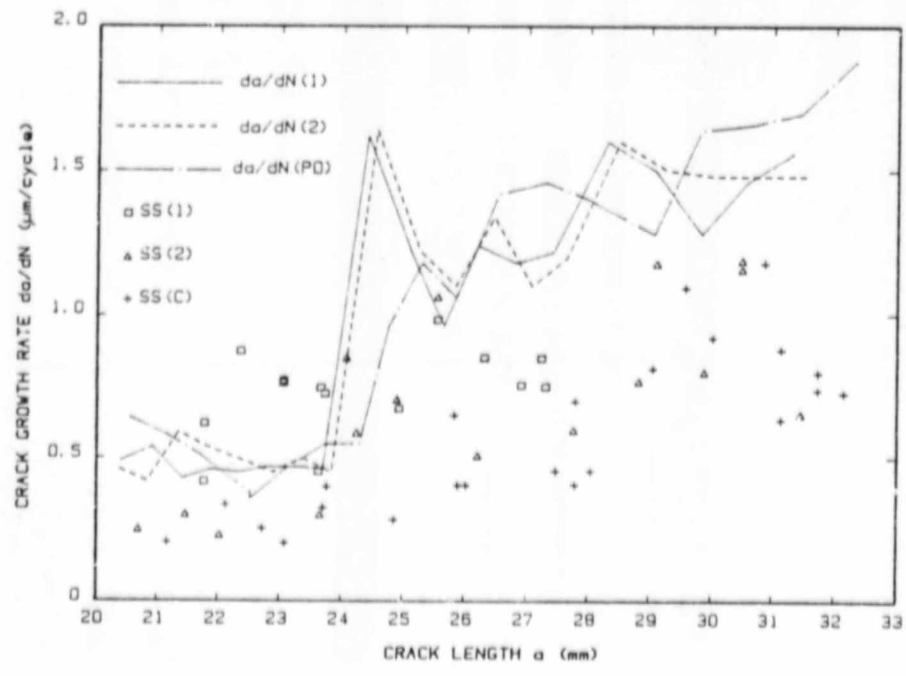

(b)

Figure 7.28 Comparison of macroscopic growth rates and striation spacing measurements in (a) specimen P4 and (b) specimen P5. Note that the striation spacing underestimates the actual growth rates, particularly at high stress intensities.